Materials Today Bio 27 (2024) 101131

Contents lists available at ScienceDirect

Materials Today Bio

journal homepage: www.journals.elsevier.com/materials-today-bio

Enhancing ovarian cancer treatment with maleimide-modified Pt(IV) prodrug nanoparticles

Yiting Bai [a], Zhenpeng Wang [a], Dongzhen Liu [a], Xiandi Meng [b,d], Haorui Wang [b,c,d], Meiling Yu [b,d], Songling Zhang [a,**], Tianmeng Sun [b,c,d,e,*]

[a] Department of Obstetrics and Gynaecology, The First Hospital, Jilin University, Changchun, Jilin, China
[b] Key Laboratory of Organ Regeneration and Transplantation of Ministry of Education, Institute of Immunology, The First Hospital, Jilin University, Changchun, Jilin, China
[c] International Center of Future Science, Jilin University, Changchun, Jilin, China
[d] National-local Joint Engineering Laboratory of Animal Models for Human Diseases, Changchun, Jilin, China
[e] State Key Laboratory of Supramolecular Structure and Materials, Jilin University, Changchun, Jilin, China

ARTICLE INFO

Keywords:
Peritoneal metastasis
Ovarian cancer
Platinum-based chemotherapy
Nanoparticle drug delivery system

ABSTRACT

The limitations of platinum in ovarian cancer therapy, such as poor solubility and significant side effects, often lead to suboptimal therapeutic outcome and mortality. In this study, we have developed a novel approach utilizing biodegradable polymeric nanoparticles as a drug delivery system (NDDS), loaded with advanced platinum (IV) (Pt(IV)) prodrugs. A key feature of our approach is the enhancement of nanoparticles with maleimide, a modification hypothesized to significantly boost tumor tissue accumulation. When tested in mouse models of orthotopic and peritoneal metastasis ovarian cancer, these maleimide-modified nanoparticles are anticipated to show preferential accumulation in tumor tissues, enhancing therapeutic efficiency and minimizing systemic drug exposure. Our findings demonstrate that the maleimide-modified Pt(IV)-loaded NDDSs significantly reduce tumor burden in comparison to traditional cisplatin therapy, while simultaneously reducing adverse side effects. This leads to markedly improved survival rates in models of peritoneal metastasis ovarian cancer, offering a promising new direction in the treatment of this challenging disease.

1. Introduction

Ovarian cancer, a critical feminine health issue, is the second most common gynecologic malignancy and a leading cause of mortality in female reproductive cancers [1]. Its insidious nature often leads to late-stage diagnosis, with a majority of patients presenting with advanced disease characterized by peritoneal metastases [2]. This scenario is particularly challenging due to the high rates of recurrence and resistance to current treatments, which significantly impacts survival outcomes [3].

The treatment landscape has long been dominated by platinum (Pt)-based drugs, ever since the introduction of cisplatin as a cornerstone of chemotherapy in 1978 [4]. Cisplatin's primary cytotoxic mechanism involves the formation of irreparable platinum-DNA adducts, resulting in significant DNA damage and subsequent induction of apoptosis. In addition, cisplatin-induced oxidative stress can lead to mitochondrial damage and dysfunction [5], depletion of glutathione (GSH) [6], lipid peroxidation [7], activation of apoptotic pathways [8], and the cumulative effect of multiple pathways culminating in apoptosis. As a result, this presents an effective therapy against malignant solid tumors. Despite their widespread use, these agents are fraught with limitations, including severe systemic side effects, cisplatin resistance, and suboptimal delivery to metastatic lesions, often resulting in inadequate treatment responses [9]. Systemic administration of cisplatin often leads to ototoxicity, neurotoxicity, hemolysis, and most notably, nephrotoxicity. Simply lowering the dosage, although could reduce side effects, inevitably results in a decreased therapeutic efficacy.

In the pursuit of overcoming these obstacles, Pt(IV) prodrugs have garnered significant interest. These prodrugs are specifically designed to overcome cellular resistance mechanisms induced by GSH and metallothionein (MT), offering a promising alternative with the potential for reduced side effects [10,11]. In addition, Pt(IV) prodrugs trigger

* Corresponding author. State Key Laboratory of Supramolecular Structure and Materials, Jilin University, Changchun, Jilin, China.
** Corresponding author.
E-mail addresses: slzhang@jlu.edu.cn (S. Zhang), tsun41@jlu.edu.cn (T. Sun).

https://doi.org/10.1016/j.mtbio.2024.101131
Received 15 April 2024; Received in revised form 6 June 2024; Accepted 16 June 2024
Available online 18 June 2024

reduction within tumor cells overexpressing GSH, enabling efficient selectively delivery of platinum-based drugs [12,13]. However, their clinical application is hampered by issues like rapid systemic absorption and distribution [14,15], and difficulty in achieving effective drug concentrations in complex tumor microenvironments [16]. Tumor microenvironments can impede drug delivery, leading to subtherapeutic concentrations and eventual resistance. Intraperitoneal (*i.p.*) therapy has emerged as a potential strategy to mitigate these issues. By administering drugs directly to metastatic site, *i.p.* therapy aims to increase local drug concentration while reducing systemic exposure [17,18]. However, this approach is hampered by premature clearance of small-sized molecules from the peritoneum, restricted distribution within the peritoneal space, and poor drug penetration in larger tumor masses [19–21].

Our study explores the use of nanoparticle (NP) technology to enhance the delivery of Pt(IV) prodrugs. Encapsulating drugs in nanocarriers serves to delay drug activation until reaching tumor tissue, thus reducing premature degradation and systemic toxicity. Additionally, tumor-targeting nanocarriers with controlled release properties can enhance drug delivery efficacy within tumor tissues. To specifically address advanced ovarian cancer, we combined intraperitoneal delivery with nanoparticle technology, aiming to deliver nano drugs that accumulated in tumors effectively, especially effective against scattered, variably sized, and poorly vascularized tumors in the peritoneal cavity. Given the association between thiol-containing species and tumor resistance, the intracellular GSH scavenging process facilitated by the liberated Pt(IV) prodrug serves a dual role, both delivering the active Pt anticancer agent and beneficial for reversing drug resistance [22,23]. This strategy seeks simultaneously tackle drug delivery barriers and concentration limitations. We developed a PEG-PLGA nanoparticle drug delivery system with and without maleimide modification (Pt(IV)@Mal-NPs and Pt(IV)@NPs), and investigated their effects on Pt(IV) prodrug distribution and tumor growth inhibition in ovarian cancer. Our findings reveal that Pt(IV)@Mal-NPs significantly improve therapeutic efficacy by promoting drug accumulation at the tumor site following *i.p.* administration.

2. Material and methods

2.1. Materials

The diblock copolymer of maleimide-grafted mPEG with PLGA (Mal-$mPEG_{5K}$-$PLGA_{10K}$) and mPEG with PLGA ($mPEG_{5K}$-$PLGA_{10K}$) were provided by J. Wang (South China University of Technology, Guangzhou, China). Platinum(IV) prodrug was purchased from Guangzhou Kelan Biotechnology Co., Ltd. (Guangzhou, China). The dulbecco's modified eagle medium (DMEM), phosphate-buffered saline (PBS), fetal bovine serum (FBS), penicillin/streptomycin, L-glutamine, 0.25 % trypsin, trypan blue, Lipofectamine 2000, 1,10-Dioctadecyl-3,3,30,30-tetramethylindodicarbocyanine, 4-chlorobenzenesulfonate salt (DiD) and Alexa Fluor (AF) 555-phalloidin were purchased from Thermo Fisher Scientific (Waltham, MA, USA). The house serum was purchased from Gibco (California, USA). DAPI Fluoromount-G was purchased from Southern Biotech (Birmingham, AL, USA). The chloroform was purchased from Yuwang Pharma (Dezhou, China). Aspartate aminotransferase assay, the urea assay kits and reduced glutathione (GSH) assay kits were purchased from Nanjing Jiancheng Bioengineering Institute (Jiangsu, China). The cisplatin was obtained from Hanson Pharma (Lianyungang, China). The propidium iodide (PI) was purchased from Solarbio Life Science (Beijing, China). The FITC Annexin V apoptosis detection kit was purchased from BD Biosciences (Franklin Lakes, NJ, USA). The enhanced cell counting kit-8 (CCK-8) and one step TUNEL apoptosis assay kit was purchased from Beyotime (Shanghai, China).

2.2. Cell lines and animals

The mouse ovarian epithelial cancer cell line (ID8) was purchased from Shanghai Institute of Materia Medica (Shanghai, China), the liver normal parenchyma cell line (NCTC1469) was purchased from American Type Culture Collection (ATCC). These cells were maintained in DMEM supplemented with 10 % FBS or horse serum and 1 % penicillin/streptomycin at 37 °C with 5 % CO_2 humidified atmosphere. BM-derived macrophages (BMDMs) were generated by flushing BM cells in the tibia and femur of C57BL/6 mice, followed by isolating and culture for induction in RPMI 1640 medium supplemented with 10 % FBS, mouse IL-4 (10 ng/ml), and M-CSF [24] for 7 days. The ID8 cells were stably transduced with green fluorescent protein (GFP) and luciferase (Luc) gene with a piggyBac transposon system. Female C57BL/6 mice and BALB/c nude mice (6–8 weeks old) were obtained from Charles River (Beijing, China) and raised in a specific pathogen-free environment with free access to food and water. Both all animals care and operating procedures used sterile techniques and performed according to the request of the Guidelines for Animal Care and Use of Laboratory Animals and Animal Ethics Committee of the First Hospital of Jilin University.

2.3. Preparation of Mal-NPs, Pt(IV)-loaded NPs and DiD-labeled NPs

Blank NPs (Mal-NPs), NPs loaded with Pt(IV), and NPs loaded with DiD were prepared by a single emulsion-solvent evaporation method.

Mal-NPs: 15 mg Mal-PEG-PLGA dissolved in 300 μL of chloroform was emulsified in 1.8 mL of double-distilled H_2O by sonication (VCX130, Sonics & Materials, Inc. Newtown, CT, USA) at 60 W for 1 min over an ice bath to form a water-in-oil emulsion, further rotary evaporated by a vacuum Rotavapor (R-210, Buchi, Flawil, Switzerland) to remove the chloroform. The NPs were collected by centrifugation (30,000×*g*, 30 min) and washed twice using sterile water to remove chloroform.

Pt(IV)-loaded NPs: 1.4 mg of Pt(IV) dissolved in 126 μL of chloroform and 14 μL of DMSO was mixed with 260 μL of chloroform containing 13.6 mg of mPEG-PLGA or Mal-mPEG-PLGA. The mixture was emulsified in 2.4 mL of double-distilled H_2O by sonication at 60 W for 1 min over an ice bath to form a water-in-oil emulsion, further rotary evaporated by a vacuum Rotavapor to remove the chloroform. NPs were collected by centrifugation (30,000×*g*, 30 min) and washed twice using sterile water to remove chloroform and possible un-encapsulated Pt(IV). The weight ratio of Pt(IV) and mPEG–PLGA or Mal-mPEG-PLGA in this preparation was 10 %.

DiD-labeled NPs: 14 μg of DiD dissolved in 14 μL of chloroform was mixed with 486 μL of chloroform containing 14 mg of mPEG-PLGA or Mal-mPEG-PLGA. The mixture was emulsified in 3 mL of double-distilled H_2O by sonication at 60 W for 1 min over an ice bath to form a water-in-oil emulsion, further procedures of rotary evaporation and collection were in accord with that of Mal-NPs.

2.4. Characterization of NPs loaded with Pt(IV) or DiD

The morphology of the Pt(IV)-loaded NPs was taken by scanning electron microscopy (SEM) at an accelerating voltage of 3.0 kV. The diameter and ζ potential of both NPs loaded with Pt(IV) or DiD were determined by a dynamic light scattering (Zetasizer NanoZS90, Malvern Instruments, UK) at 25 °C. The supernatant of centrifugation during NPs preparation was lyophilized and dissolved in aqua regia to determine the drug loading capacity of Pt(IV) in Pt(IV)@NPs and Pt(IV)@Mal-NPs using an inductively coupled plasma mass spectrometer (iCAP Q, Thermo Fisher, Waltham, MA, USA). The un-encapsulated Pt was expressed as the Pt concentration in the supernatant. The drug encapsulation percentage was calculated as follows: drug encapsulation percentage = (1-wt of un-encapsulated drug/total weight of drug) × 100 %.

2.5. Cargo release from NPs loaded with Pt(IV) or DiD in vitro

The cargo release behaviors of Pt(IV)-loaded NPs and DiD-labeled NPs were both investigated *in vitro* by the dynamic analysis method. As an example, an aliquot of these NPs aqueous solution was injected into dialysis bags (3.5 kDa MWCO, Shanghai yuanye Bio-Technology Co., Ltd), then immersed in 20 mL sterile water (pH 7.4) on a constant temperature horizontal shaker at 37 °C. At different time intervals, the release solution was collected, and immediately using an equal volume of sterile water instead. The concentration of Pt was measured by ICP–MS analysis. The Pt released from NPs was expressed as the total Pt released out of the dialysis bag. The difference for DiD-labeled NPs was that an equal volume of the DiD-labeled NPs solution from the dialysis bag was transferred to a 96-well plate at each time point, and the absorbance at 640 nm was measured using a multifunctional microporous plate autoanalyzer (Spark, TECAN, Mannedorf, Zurich, Switzerland) to calculate the cumulative fluorescence signal release of DiD-labeled NPs over 24 h.

2.6. Cell viability assays

The cellular viability was evaluated via CCK-8 assays. ID8 cells, ID8-luc/GFP cells, or NCTC1469 were seeded into 96-well plates (4×10^3 cells/well) and incubated overnight, while BMDMs were generated using the isolated BM cells, as described above, and were further seeded into 96-well plates (2×10^4 cells/well) and cultured for 7 days' induction. The cells per well were further exposed to 100 μL culture medium containing CisPt, Pt(IV), Mal-NPs, Pt(IV)@NPs, and Pt(IV)@Mal-NPs for 48 h at different final Pt concentrations. Cells cultured in complete medium with isochoric PBS were used as the control. Subsequently, added 10 μL CCK-8 solution to each well and incubated for 2 h at 37 °C. The cell viability was measured according to the OD value at 450 nm via a multifunctional microporous plate autoanalyzer. The IC50 values of drugs were analyzed with GraphPad software.

2.7. Cellular uptake assays

ID8 cells were seeded into 24-well plates (1×10^5 cells/well) and incubated overnight. The cells per well were incubated with PBS, 0.05 μM, 0.5 μM, 5 μM, 50 μM DiD@NPs, and DiD@Mal-NPs suspended at 37 °C for 24 h. The medium was removed and cells were collected after rinsed twice with cold PBS. The fluorescence intensity was determined by flow cytometry (LSRFortessa, BD Bioscience, San Jose, CA, USA). The data were analyzed with FlowJo software (TreeStar, San Carlos, CA, USA).

For fluorescence microscopy observation, 2×10^4 of ID8 cells/well were seeded into 24-well plates loaded with a coverslip and incubated overnight, then treated with culture medium containing PBS, 50 μM DiD@NPs, and DiD@Mal-NPs for 24 h. Isochoric in complete medium was used as controls. The medium was removed and cells were washed twice with cold PBS, followed by fixation with 4 % paraformaldehyde for 30 min at 25 °C.

The nuclei and cytoskeleton were stained with DAPI and FITC respectively according to the manufacturer's instructions. The uptake of NPs was observed by laser scanning confocal microscope (LSM 880, Zeiss, Jena, Germany).

2.8. Apoptosis analysis

ID8 cells were seeded into 24-well plates (2×10^4 cells/well) and incubated overnight. PBS, 5 μM Pt(IV)@NPs, and 5 μM Pt(IV)@Mal-NPs were added and cultured for 48 h.

The apoptotic cells were examined by a FITC Annexin V apoptosis detection kit. Briefly, cells were washed with cold PBS twice and further resuspended in 100 μl binding buffer at a concentration of 1×10^6, incubated for 15 min at 25 °C in the dark after added 5 μl FITC Annexin V and 5 μl PI. Subsequently, 400 μl binding buffer was added to each tube. Finally, apoptotic cells were examined by flow cytometry, and the data were analyzed by FlowJo software. Annexin FITC Annexin V^+/PI^- represented early apoptotic cells, FITC Annexin V^+/PI^+ represented late apoptotic cells, and FITC Annexin V^-/PI^+ represented necrotic cells.

2.9. GSH detection

ID8 cells were seeded into 24-well plates (2×10^4 cells/well) and incubated overnight. PBS and 5 μM Pt-based drugs (CisPt, Pt(IV), Mal-NPs, Pt(IV)@NPs, and Pt(IV)@Mal-NPs) were added and cultured for 48 h. After the cells were collected and washed with PBS three times, the GSH concentration of the samples was determined by a reduced GSH assay kit, and was expressed as μmol GSH per g protein.

2.10. Peritoneal metastasis tumor model establishment

The animal experiments involved in this study were approved by the Animal Ethics Committee of the First Hospital of Jilin University. For establishment of the intraperitoneal (*i.p.*) tumor models, C57BL/6 mice ($n = 3$) received 1×10^7 luciferase/GFP-expressing ID8 (ID8-luc/GFP) cells suspended in 200 μL PBS by *i.p.* injection into the peritoneal cavity. 21 days post inoculation with ID8 cells, mice were received D-luciferin firefly potassium salt via *i.p.* injection at a dose of 150 mg/kg and imaged using the IVIS Spectrum imaging system (PerkinElmer, Waltham, USA).

2.11. Orthotopic xenograft experiments

For an orthotopic ovarian tumor model, BALB/c Nude mice were anesthetized by subcutaneous injection of 5×10^6 ID8-luc/GFP cells in a mixture of 100 μL PBS and 100 μL Matrigel 14 days ago. Then the mouse was sacrificed for isolating tumor (volumes~ 4 mm^3).

Following anesthetizing, C57BL/6 mice ($n = 3$) were local shaved on the right dorsum and placed on their right side. The operation of orthotopic xenografting was under the micro magnifier as described [25]. The tumor growth was evaluated via bioluminescence imaging (BLI).

2.12. In vivo biodistribution of DiD-labeled NPs

For IVIS imaging, intraperitoneal tumor-bearing or orthotopic tumor-bearing C57BL/6 mice were *i.p.* injected with NPs loaded with DiD or PBS as control in the lower left quadrant. The dose of NPs was 227 mg per kg mouse body weight. D-luciferin potassium salt was intraperitoneally injected with at a dose of 1.5 mg/kg 10 min before imaging. The parameters of near-infrared (NIR) fluorescence image were set based on DiD at an excitation (Ex) wavelength of 640 nm and an emission (Em) wavelength of 700 nm. Main organs of C57BL/6 mice (brains, hearts, lungs, livers, spleens, kidneys, uteruses and adnexa, diaphragms, mesenteries and peritonea) were taken at 24 h after DiD-labeled NPs administration via the IVIS Spectrum system. The Data were analyzed using the Living Image software (PerkinElmer, Waltham, MA, USA).

For fluorescence microscopy observation, the mouse organs were fixed in 4 % paraformaldehyde (PFA) for 24 h and then immersed in 30 % sucrose solution. Suddenly, organs frozen in Optimal Cutting Temperature (O.C.T.) compound were cut into 5-μm sections and stained with AF555-phalloidin for 1 h at 4 °C in dark. After counterstained with DAPI, the cellular uptake of DiD-labeled NPs was visible under a LSM880 (Zeiss).

2.13. Tissue distribution and tumor accumulation of Pt(IV)-loaded NPs

In the peritoneal tumor model, either CisPt, Pt(IV)@NPs, and Pt(IV)@Mal-NPs were *i.p.* injected into C57BL/6 mice at a dose of 4 mg Pt per

kg mouse body weight after 21 days post inoculation with ID8 cells. Main celiac organs (livers, kidneys, diaphragms, mesenteries and peritonea) were taken at 24 h after drugs administration for ICP-MS analysis.

For orthotopic ovarian tumor model, C57BL/6 mice were *i.p.* injected with CisPt, Pt(IV), Pt(IV)@NPs, and Pt(IV)@Mal-NPs at the same dose (Pt 4 mg/kg) after 14 days post tumor transplanting. Representative targeting organs (livers, kidneys, diaphragms, peritonea, uteruses with left ovaries, right ovaries) were taken at 24 h after drugs administration for ICP-MS analysis.

The isolated tissues were weighed and weighed again after cut into above 200 mg pieces, then completely reacted with nitric acid (0.50 ml) and hydrogen peroxide (20 μl) at 120 °C. Homogenized samples were dissolved in aqua regia [nitric acid and hydrochloric acid (1:3, v/v)], then diluted by deionized water and filtered twice before ICP-MS analysis (iCAP Q, Thermo Fisher, Waltham, MA, USA).

2.14. In vivo therapeutic study

For antitumor efficacy evaluation, C57BL/6 mice bearing ID8-luc/GFP ovarian cancer intraperitoneal models were divided randomly into 5 groups (n = 5) as PBS, CisPt, Mal-NPs, Pt(IV)@NPs, and Pt(IV)@Mal-NPs, and intraperitoneally injected at doses of 0.4, 1, or 4 mg Pt/kg body weight once a week for 4 times. Tumor growth was determined by the IVIS Spectrum system before injections and sacrificed. To monitor potential toxicity, all mice were measured for signs of weight loss or abdominal distention once a week. Animals were euthanized at the endpoint when the peritoneal tumor nudes and ascitic volume were counted, plasma and the major organs were collected. The body weight, liver weight and kidney weight of mice were measured. The survival rate of mice in every group was observed.

2.15. Hematological analysis and biochemical parameters

Blood cells were counted via ProCyte Dx Hematology Analyzer (IDEXX laboratories Inc., USA). The aspartate aminotransferase (AST) and blood urea nitrogen (BUN) were evaluated using specific assay kits for respectively monitoring liver function and kidney function in a multifunctional microporous plate autoanalyzer.

2.16. Tissue histopathology and apoptosis analysis

The main organs (livers, kidneys, diaphragms, mesenteries and peritonea) were harvested and fixed in 4 % paraformaldehyde. After sliced into 2.5-μm-thick sections, besides ovaries in orthotopic ovarian tumor model were stained with one step TUNEL apoptosis assay kit according to the instruction, all tissues were stained with hematoxylin and eosin. The sections were examined by a LSM880 or an optical microscope (IX71, Olympus, Tokyo, Japan).

2.17. Statistical analysis

All data are presented as mean ± standard deviation. Statistics were analyzed by the Student's t-test for two groups and one-way analysis of variance for multiple groups on GraphPad Prism 8. P values < 0.05 (*) were considered statistically significant, and P values < 0.01 (**) were considered statistically significant extremely.

3. Results

3.1. Enhanced drug delivery efficiency in PLGA-based nanoparticles with maleimide modification

In our research, we successfully synthesized biocompatible poly (ethylene glycol) (PEG)–PLGA–based nanoparticles with or without maleimide modification loaded with Pt(IV) using a single emulsion method. This included both standard Pt(IV)-loaded NPs (Pt(IV)@NPs) and maleimide-modified versions(Pt(IV)@Mal-NPs), with the drug encapsulated within their hydrophobic cores (Fig. 1A). The hydrodynamic diameters, as measured by dynamic light scattering (DLS), were 181.3 ± 4.3 nm for Pt(IV)@NPs and 275.6 ± 5.0 nm for Pt(IV)@Mal-NPs, with ζ potentials of −27.4 ± 1.2 mV and −26.6 ± 0.9 mV, respectively (Fig. 1B and C). Scanning electron microscopy (SEM) revealed that both types of NDDSs maintained a consistent spherical morphology (Fig. 1D). The efficiency of Pt(IV) encapsulation was high, as indicated by minimal Pt detected in the supernatants via inductively coupled plasma-mass spectrometry (ICP-MS). The drug encapsulation efficiency at different drug feeding ratios were detailed in Table 1. For further experiments, the 10 % Pt to PEG-PLGA (or Mal-PEG-PLGA) feed mass ratio was chosen for both Pt(IV)@NPs and Pt(IV)@Mal-NPs, due to its effectiveness. Drug release profiles in deionized water (pH 7.4) at 37 °C showed sustained drug release over 96 h, with a cumulative release exceeding 20 % (Fig. 1E).

In assessing the antitumor efficacy of our nano-formulations, we conducted cell uptake assays on ID8 cells with DiD-labeled PEG–PLGA-based (DiD@NPs) and maleimide-modified Mal-PEG–PLGA-based nanoparticles (DiD@Mal-NPs), synthesized similarly to Pt(IV)-loaded NDDSs. The hydrodynamic diameters of DiD@NPs and DiD@Mal-NPs were 160.3 ± 2.6 nm and 258.8 ± 5.9 nm, respectively, with their respective ζ potentials measured at −21.9 ± 1.6 mV and −21.6 ± 1.3 mV, as illustrated in Fig. S1. Flow cytometry (FCM) analysis over 4 and 24 h revealed time-dependent uptake for both NDDS types (Fig. S2A). Notably, DiD@Mal-NPs demonstrated significantly higher cellular internalization than DiD@NPs at both time intervals (39.8 % vs 27.1 %, $p < 0.05$ for 4 h; 93.4 % vs 74.1 %, $p < 0.0001$ for 24 h). Moreover, for a 48 h study, ID8 cells co-cultured with varying doses of DiD@Mal-NPs exhibited the highest level of intracellular fluorescence compared to other groups (Fig. 2A). Confocal laser scanning microscopy (CLSM) further visualized this uptake, showing stronger fluorescence intensity for DiD@Mal-NPs (Fig. 2B), corroborated by a markedly right-shifted peak plot of the DiD fluorescence channel in FCM analysis (Fig. S2B), suggesting enhanced uptake efficiency.

3.2. Mal-NPs showed enhanced accumulation ability in both orthotopic and peritoneal metastasis ovarian cancers

To assess the biodistribution of our nano-formulations, stable luciferase expressing ovarian cancer cells, ID8-luc/GFP, were utilized. This approach allowed visualization of ID8 cells with IVIS imaging after administrating the substrate (luciferin) via intraperitoneal injection. We labeled NPs with DiD fluorescence and confirmed its stable binding (Fig. S3). Fig. 3A illustrates the experimental procedure on C57BL/6 mice which received cancer cells injection into the abdominal cavity. Using IVIS imaging to track the DiD fluorescent signal, we observed consistent detection of DiD@NDDSs within 24 h post-injection, with increased accumulation over time (Fig. 3B). Notably, DiD@Mal-NPs exhibited significantly heightened fluorescent signals, particularly within peritoneal tissues such as the peritoneum, diaphragm, and mesentery, which are typically associated with ovarian cancer metastases. This pattern was more pronounced compared to non-targeted organs (such as the lung, liver, spleen, and kidney) (Fig. 3C), indicating that maleimide-modification enhances nanoparticle accumulation in tumor tissues rather than in major organs. This is further supported by immunofluorescence staining which demonstrated distinct DiD fluorescence in the peritoneum (Fig. 3D), mesentery (Fig. S4A), and diaphragm (Fig. S4B) of mice treated with DiD@Mal-NPs, while no significant difference in the DiD signal intensity in the liver (Fig. S4C) and kidney (Fig. S4D) across DiD@NPs, DiD@Mal-NPs, and PBS groups.

The concentrations of Pt in various tissues were analyzed using ICP-MS. Unlike cisplatin (CisPt) which demonstrated much higher accumulation in normal organs compared to tumor associated tissues, Pt(IV)@Mal-NPs treated group exhibited preferred distribution within peritoneum, diaphragm and mesentery, suggesting a potential reduction in

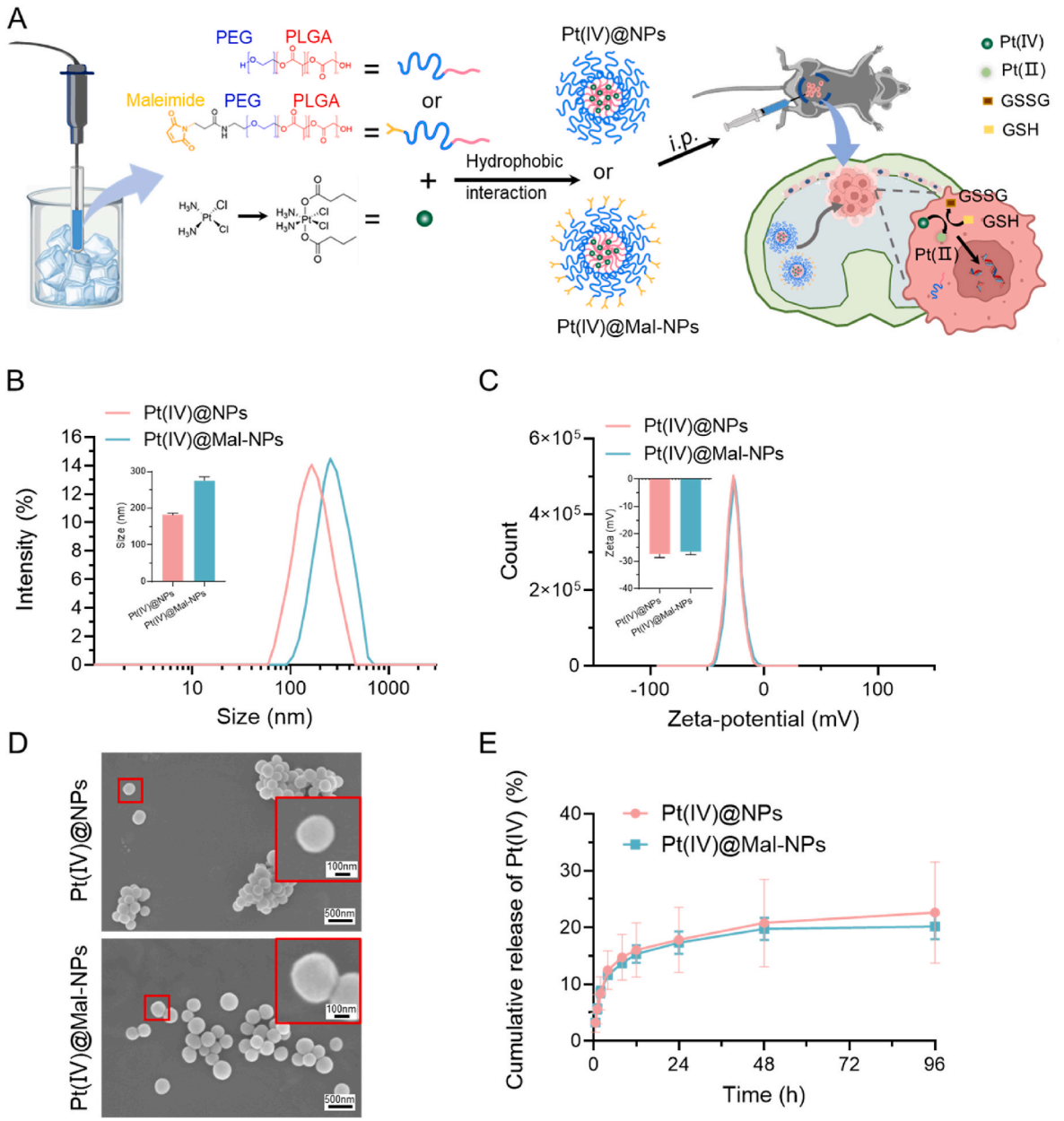

Fig. 1. Synthesis and characterizations of NPs loaded with Pt(IV). (A) Synthesis and fabrication of Pt(IV)@NPs and Pt(IV)@Mal-NPs. (B and C) Intensity distribution of the particle size (B) and zeta potential (C) of Pt(IV)@NPs and Pt(IV)@Mal-NPs determined by dynamic light scattering (n = 3). (D) SEM imaging of NPs loaded with Pt(IV)with a drug inventory ratio of 10 %. Scale bar, 500 nm, 100 nm. (E) Drug release evaluation of Pt(IV)@NPs and Pt(IV)@Mal-NPs *in vitro* (n = 3). Data are presented as the means ± SEM. *p < 0.05.

Table 1
Characterization of characterization of Pt(IV)-loaded NPs.

%DFR	NPs loaded with Pt(IV)					
	5 %		10 %		20 %	
Materials	PEG-PLGA	Mal-PEG-PLGA	PEG-PLGA	Mal-PEG-PLGA	PEG-PLGA	Mal-PEG-PLGA
Size(nm)	206.5 ± 2.0	380.4 ± 8.5	181.3 ± 4.3	275.6 ± 5.0	150.9 ± 3.3	514.3 ± 11.5
Zeta (mV)	−28.8 ± 0.8	−28.5 ± 0.3	−27.4 ± 1.2	−26.6 ± 0.9	−24.5 ± 0.1	−23.5 ± 0.2
%EE	86.0	83.2	87.7	90.3	89.8	90.0

DFR: drug feeding ratio; EE: encapsulation efficiency.

systemic toxicity (Fig. 3E). Remarkably, the Pt levels were significantly higher in this group than the Pt(IV)@NPs group, indicating more effective targeting of tumor tissues (Fig. 3E). This pattern aligns with IVIS findings, suggesting that maleimide-modified nanoparticles preferentially target tumor tissues, indicating potential enhanced biosafety compared to traditional CisPt treatments.

C57BL/6 mice with orthotopic transplantation of ovarian tumors were applied to further assess the tumor targeting nature of NPs (Fig. 4A). The well-established animal models were confirmed by observation of luciferase signal from *ex vivo* imaging using IVIS (Fig. S5). Notably, the DiD@Mal-NPs treated group compared to DiD@NPs has demonstrated enhanced fluorescence in the lung, spleen, and tumor lesions (Fig. 4B). As well as more robust fluorescence in the tumor than the normal ovary (Fig. 4C). Quantitative Pt analysis showed Pt(IV)@Mal-NPs had higher Pt concentrations in the tumor-bearing right

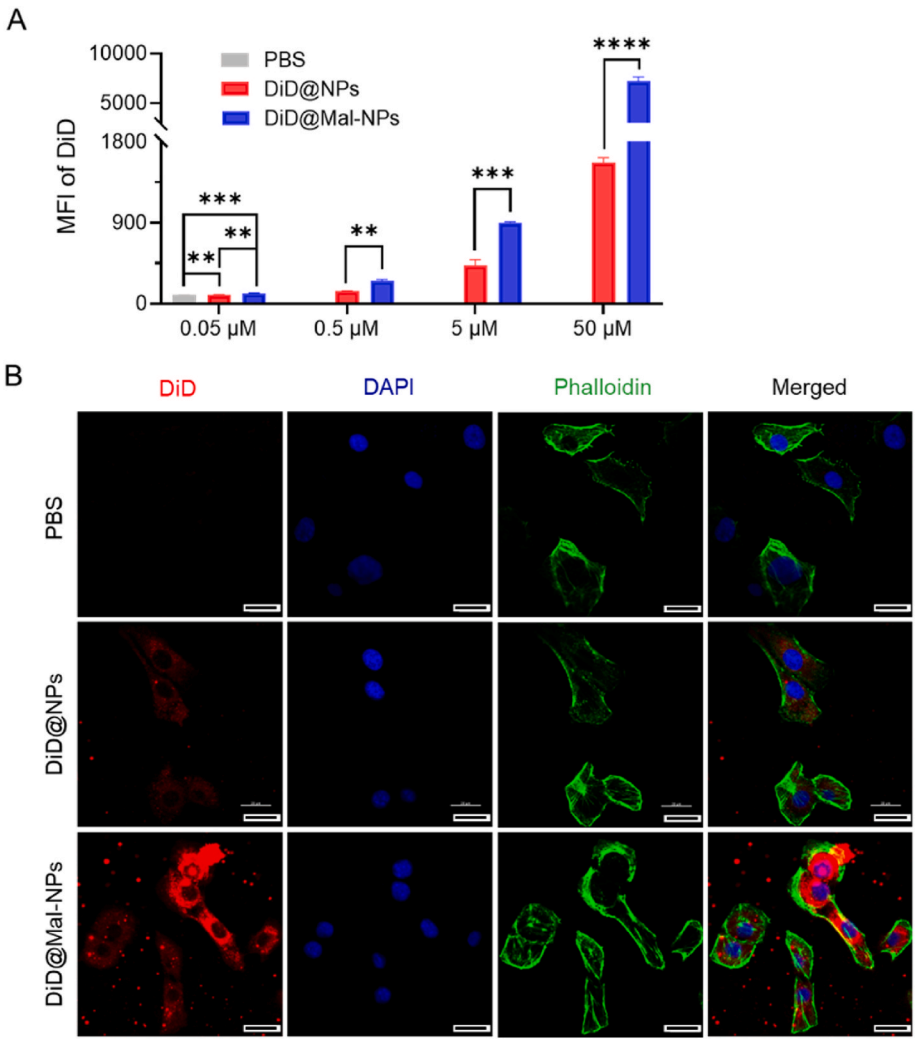

Fig. 2. The maleimide modification significantly enhances the cellular uptake of NPs *in vitro*. (A) Flow cytometry analysis of the relative mean fluorescence intensities (MFI) of DiD in ID8 cells after treatment with various doses of PBS, DiD@NPs, and DiD@Mal-NPs at 37 °C for 48 h (n = 3). (B) Representative confocal laser scanning microscopy (CLSM) images of ID8 cells after 24 h incubation with PBS, DiD@NPs, and DiD@Mal-NPs at 37 °C. The cytoskeleton and nuclei were stained with AF555-phalloid (green) and DAPI (blue), respectively. Scale bar, 20 μm. Data are presented as the means ± SEM. *$p < 0.05$, **$p < 0.01$, ***$p < 0.001$, ****$p < 0.0001$. (For interpretation of the references to color in this figure legend, the reader is referred to the Web version of this article.)

ovary, with values of 2.5 μg/g for Pt(IV)@Mal-NPs, 2.1 μg/g for Pt(IV)@NPs, 1.5 μg/g for Pt(IV), and 1.8 μg/g for CisPt (Fig. 4D). However, in non-target tissues, Pt concentrations for Pt(IV)@NPs and Pt(IV)@Mal-NPs were considerably lower than CisPt (Fig. 4D). H&E and TUNEL staining indicated that Pt(IV)@Mal-NPs induced significant apoptosis in ovarian cancer, suggesting effective tumor site accumulation and potential therapeutic advantage (Fig. 4E).

3.3. *Pt(IV)@Mal-NPs enhanced the antitumor efficiency of Pt(IV) both in vitro and in vivo*

Leveraging the targeted accumulation benefit of maleimide-modified nanoparticle drug delivery systems (Pt(IV)@Mal-NPs), we evaluated their antitumor efficacy as drug carriers against ovarian tumor. First of all, ID8 cells were treated with various concentrations of CisPt, Pt(IV), Mal-NPs, Pt(IV)@NPs, and Pt(IV)@Mal-NPs for 48 h. As shown in Fig. 5A, both Pt(IV)@NPs and Pt(IV)@Mal-NPs formulations had superior inhibitory effects on ID8 cell proliferation compared to CisPt, with an IC50 value of 0.4 μM, significantly lower than CisPt's 7.0 μM. Similarly, a consistent phenomenon was observed in ID8-luc/GFP cells (Fig. S6). Notably, Pt(IV)@Mal-NPs demonstrated enhanced therapeutic efficacy, highlighting the significant improvement in treatment outcomes for peritoneal metastatic ovarian cancer cells due to maleimide modification.

To further evaluate whether the toxic effect of Pt(IV) formulated NPs restricted to cancer cells rather than normal cells, BMDMs and NCTC1469 were treated with various platinum-containing NPs at different drug concentrations, which respectively represented the normal cell type with relatively stable growth characteristics and physiological states, and the liver normal parenchyma cells characterized by high glutathione content. While the cell proliferation of ID8 cells significantly inhibited by Pt(IV)@NPs and Pt(IV)@Mal-NPs as the Pt concentration increased, both BMDMs and NCTC1469 cells remained viable (Fig. 5B), indicating that both formulations enable a selective cytotoxic towards ovarian cancer cells.

Flow cytometer (FCM) and apoptosis staining revealed that Pt(IV)-loaded NPs, especially those modified with maleimide, induced higher rates of apoptosis in ID8 cells (Fig. 5C). Furthermore, the rates of early and late apoptosis were remarkably increased in both Pt(IV)@NPs and Pt(IV)@Mal-NPs treated group in comparison to CisPt ($p < 0.0001$); while significance also existed within nanoformulations, Pt(IV)@Mal-NPs showed enhanced effects compared to Pt(IV)@NPs (33.40 % vs 12.40 %, $p < 0.0001$ in the early apoptosis rate; 29.33 % vs 18.93 %, $p < 0.01$ in the late apoptosis rate) (Fig. 5D and E). These results suggest that

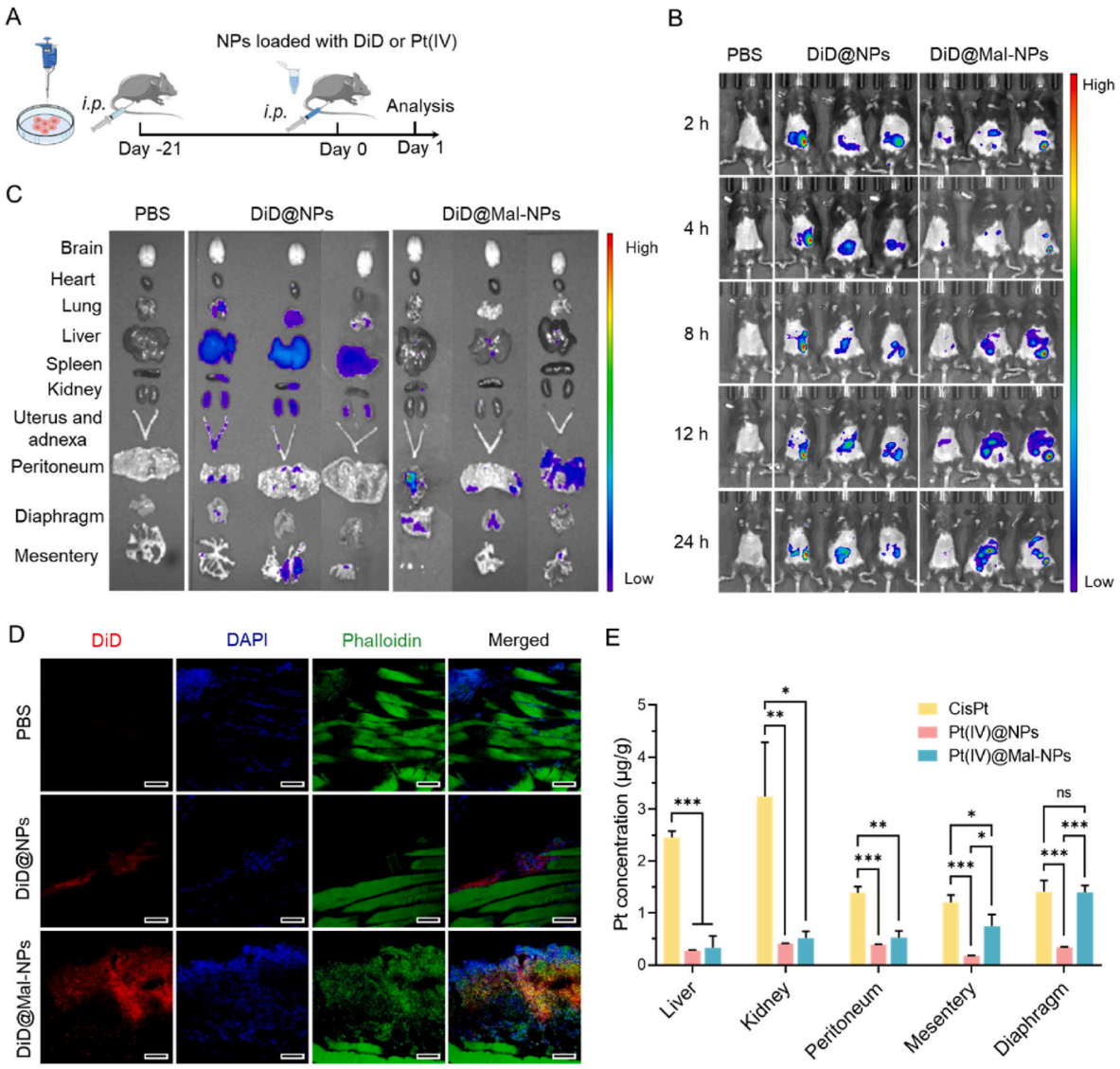

Fig. 3. Improved drug delivery efficiency *in vivo*. (A) Schematic diagram depicting the establishment of the peritoneal metastasis tumor model and the procedure for *in vivo* biodistribution studies. (B) *In vivo* fluorescent imaging of C57BL/6 mice with peritoneal metastasis ID8-luc tumors after *i.p.* injection of PBS, DiD@NPs, and DiD@Mal-NPs at different time points. (C) *Ex vivo* fluorescent imaging at 24 h post-injection. (D) CLSM images demonstrate the distribution of DiD-labeled NPs in the peritoneum of peritoneal metastasis tumor-bearing mice at 24 h after administration. The cytoskeleton and nuclei were stained with AF555-phalloid (green) and DAPI (blue), respectively. Scale bar, 50 μm. (E) ICP-MS analysis demonstrates the retention of 50 μm CisPt, 50 μm Pt(IV)@NPs, and 50 μm Pt(IV)@Mal-NPs in major organs of peritoneal metastasis tumor-bearing mice at 24 h post-treatment (n = 3).Data are presented as the means ± SEM. *$p < 0.05$, **$p < 0.01$, ***$p < 0.001$. (For interpretation of the references to color in this figure legend, the reader is referred to the Web version of this article.)

Pt(IV)-loaded NPs are capable to promote apoptosis in ovarian cancer cells, with a more pronounced effect observed when the nanoparticles are modified with maleimide.

In addition, the GSH levels in all treatment groups were determined using a GSH detection kit to investigate the impact of GSH-responsive processes on cytotoxicity *in vitro* in ID8 cells. The GSH contents in both Pt(IV)@NPs and Pt(IV)@Mal-NPs groups were found to be significantly reduced (~40 %, $p < 0.0001$) compared to the Pt(IV) group (Fig. 5F).

As the majority of ovarian cancer patients are diagnosed at an advanced stage with widespread metastasis, we established peritoneal metastatic ovarian cancer model on mice to investigate the therapeutic effects of Pt(IV)@NPs. Mice bearing peritoneal metastasis tumor derived from ID8-luc/GFP cells were subjected to treatment with PBS, Mal-NPs, Pt(IV), Pt(IV)@NPs, and Pt(IV)@Mal-NPs at a dosage of 4 mg Pt/kg body weight per week for 4 cycles through intraperitoneal delivery (Fig. 6A). IVIS monitoring over 28 days revealed significant bioluminescence distinguishes, representing tumor clearance, in mice receiving Pt(IV)@NPs and Pt(IV)@Mal-NPs compared to PBS, neat Mal-NPs or CisPt (Fig. 6B). Discrepancies in average fluorescence intensities *in vivo* were illustrated in Fig. S7 showing a decreasing tendency for Pt(IV)@NPs and Pt(IV)@Mal-NPs. Such effects on inhibiting tumor growth was further confirmed by the survival investigation demonstrating remarkable prolonged survival of mice treated with Pt(IV)-loaded NPs (all alive >120 days) (Fig. 6C) In addition, abdominal tumors in mice treated with Pt(IV)-loaded NPs exhibited a significant decrease ($p < 0.0001$) compared to the PBS and Mal-NPs groups, and even notably less than the CisPt group (Fig. 6D).This was consistent with the minimal tumor metastasis areas revealed in H&E staining within the abdominal cavity (Fig. 6E). Together, these results underscore the pivotal role of Pt(IV)-loaded NPs in enhancing anti-tumor efficacy and extending survival, highlighting the substantial potential of combining intraperitoneal administration with platinum-based prodrug NPs to improve therapeutic outcomes in abdominal metastatic ovarian cancer.

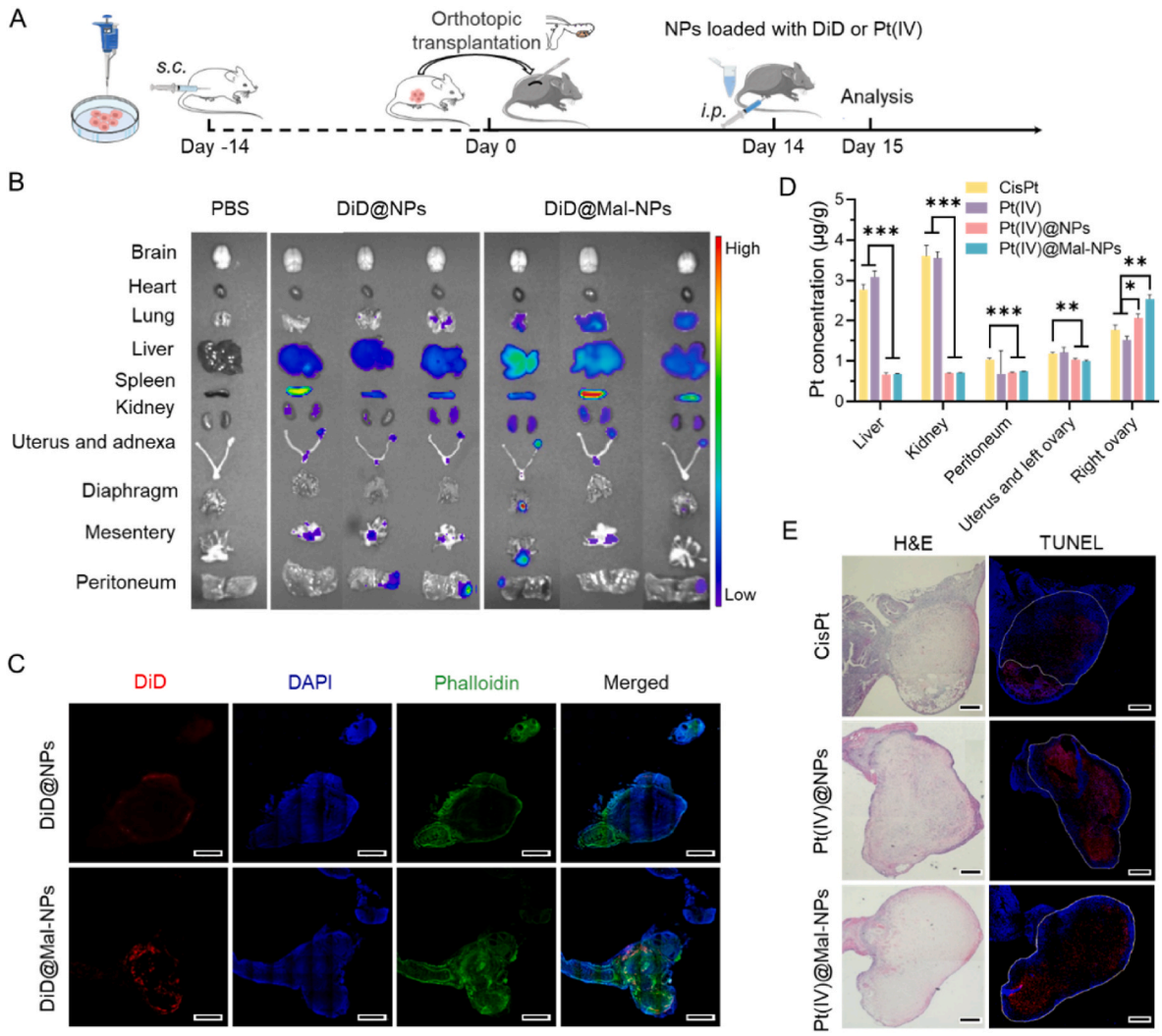

Fig. 4. ***In vivo* tumor targeting.** (A) Schematic diagram illustrating the establishment of the orthotopic tumor model and the procedure for *in vivo* tumor targeting studies. (B) Biodistribution of DiD@NPs *ex vivo* at 24 h post-injection. (C) Representative images of confocal fluorescence demonstrating the distribution of DiD-labeled NPs in the tumor site of orthotopic ovarian cancer 24 h post-injection. The cytoskeleton and nuclei were stained with AF555-phalloid (green) and DAPI (blue), respectively. Scale bar, 500 μm. (D) ICP-MS analysis of Pt levels in major organs and tumors of orthotopic tumor-bearing mice at 24 h after *i.p.* injection with 50 μm CisPt, 50 μm Pt(IV), 50 μm Pt(IV)@NPs, and 50 μm Pt(IV)@Mal-NPs (n = 3). (E) Representative images of H&E, and TUNEL immunohistofluorescence staining demonstrating the apoptotic status (red) within the orthotopic transplanted tumor tissues at 24 h post-injection of CisPt, 50 μm Pt(IV)@NPs, and 50 μm Pt(IV)@Mal-NPs. The cytoskeleton and nuclei were stained with DAPI (blue), respectively. Scale bar, 500 μm. Data are presented as the means ± SEM. *p < 0.05, **p < 0.01, ***p < 0.001. (For interpretation of the references to color in this figure legend, the reader is referred to the Web version of this article.)

Considering the promising biodistribution and tumor targeting outcomes of Pt(IV)@Mal-NPs, we conducted further investigations to compare the differential therapeutic efficacy of the two Pt(IV)-loaded nano-formulations at lower drug doses, 1 mg or 0.4 mg Pt/kg body weight using the same tumor model and treatment procedures as illustrated in Fig. 6A. Following with the Guidelines for Animal Care and Use of Laboratory Animals, the control PBS group was excluded since the experimental conditions for the group remained consistent with previous experiments. Encouragingly, the Pt(IV)@Mal-NPs exhibited superior therapeutic effects on tumor growth, as monitored by IVIS imaging, particularly in mice receiving doses of 1 mg Pt/kg body weight (Fig. 7A and B). On day 28 after treatment, all animals were sacrificed, and the abdominal tumors and ascites were quantified respectively to evaluate the therapeutic efficacy (Fig. 7C and D). Consistent with the tumor growth patterns, the Pt(IV)@Mal-NPs group at both doses displayed fewer tumor nodules and reduced ascites volumes compared to the Pt (IV)@NPs group. Histological examination using H&E staining of the peritoneum, mesentery, and diaphragm confirmed these therapeutic outcomes (Fig. 7E), indicating that at lower doses, Pt(IV)@Mal-NPs had remarkable therapeutic efficacy against peritoneal ovarian cancer and superior tumor inhibition compared to Pt(IV)@NPs, primarily due to enhanced intratumor drug accumulation. Collectively, these findings highlight he significant improvements in *in vivo* therapeutic efficacy of NPs achieved through maleimide modification of PEG end-groups, which become more pronounced at lower therapeutic doses.

3.4. Therapeutic toxicity study in vivo

An assessment of the off-target toxicity of the nanoformulations was conducted by monitoring variations in body weight, biochemical parameters, blood cell counts, and histopathology. The body weight of all groups was monitored weekly throughout the experiment. All treatment groups demonstrated marginal changes in body weight, indicating good tolerance to the nano-formulations (Fig. 8A). Subsequently, complete blood counts (CBC) were analyzed (Fig. 8B–D), and biochemical parameters were assessed via serology in all groups (Fig. 8E and F). The treatment with CisPt led to a significant decrease in WBC ($p < 0.05$) and PLT ($p < 0.01$) levels, along with a noticeable increase in BUN levels,

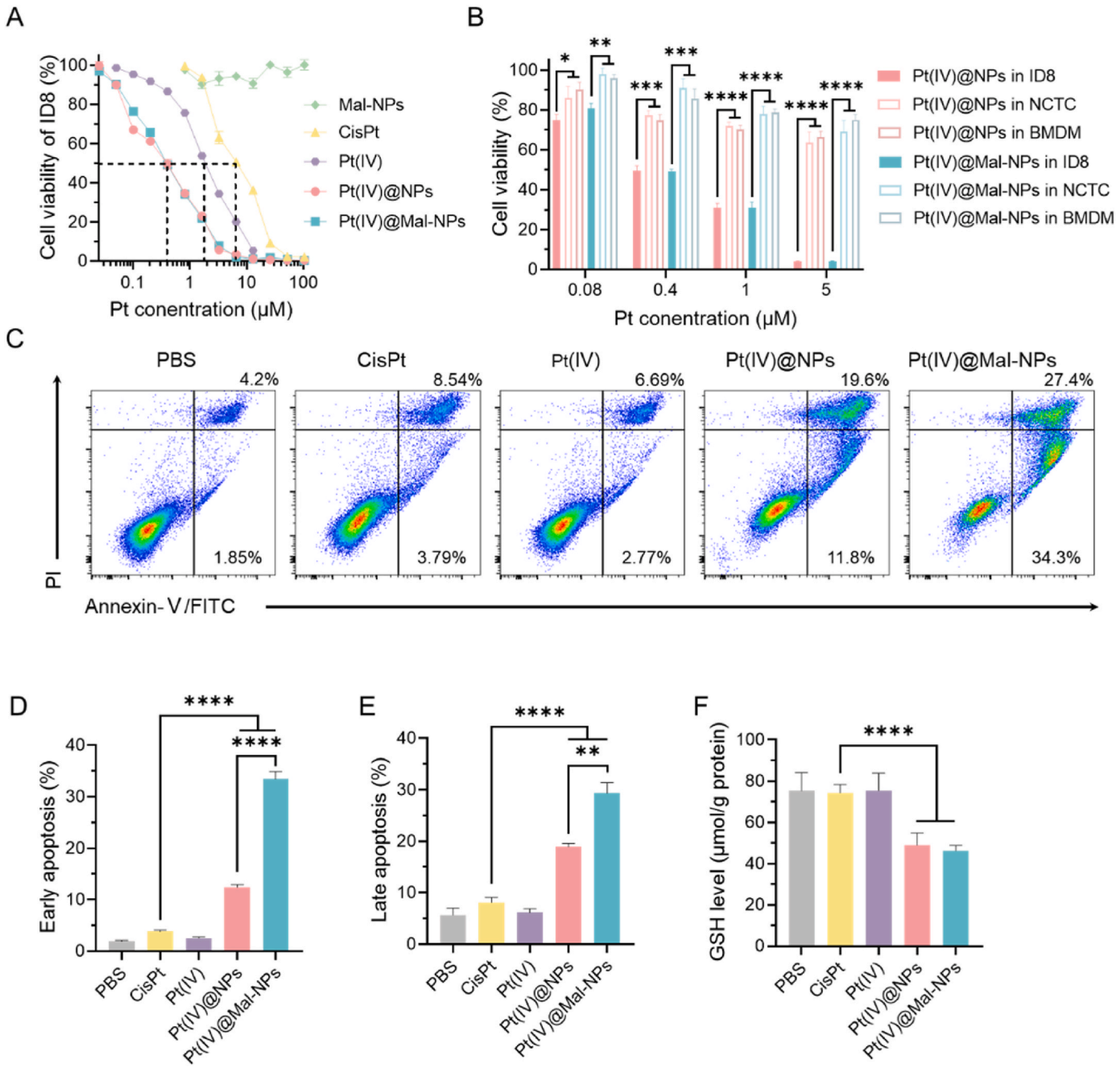

Fig. 5. ***In vitro*** **evaluation of the antitumor efficacy of NPs loaded with Pt(IV)** ***in vitro***. (A) Cytotoxicity study conducted on ID8 ovarian cancer cells using different concentrations of CisPt, Pt(IV), Mal-NPs, Pt(IV)@NPs, and Pt(IV)@Mal-NPs for 48 h (n = 3). (B) Cell viabilities of ID8 ovarian cancer cells, BMDMs, and NCTC1469 liver normal parenchyma cells at different concentrations of Pt(IV)@NPs and Pt(IV)@Mal-NPs for 48 h (n = 3). (C) Representative flow cytometry plots illustrating apoptotic cells (right) and the frequency of live cells (left) in ID8 cells following incubation with PBS, 5 μM CisPt, 5 μM Pt(IV), 5 μM Pt(IV)@NPs, and 5 μM Pt(IV)@Mal-NPs for 48 h (n = 3). (D and E) Assessment of early apoptosis (D) and late apoptosis (E) in ID8 cells treated with PBS, 5 μM CisPt, 5 μM Pt(IV), 5 μM Pt (IV)@NPs, and 5 μM Pt(IV)@Mal-NPs for 48 h (n = 3). (F) Measurement of GSH levels in ID8 cells after treatment with PBS, 5 μM CisPt, 5 μM Pt(IV), 5 μM Pt(IV) @NPs, and 5 μM Pt(IV)@Mal-NPs for 48 h (n = 3). Data are presented as the means ± SEM. *p < 0.05, **p < 0.01, ***p < 0.001, ****p < 0.0001.

indicating kidney function damage compared to other four groups. Furthermore, histopathological examination revealed edema and focal necrosis of hepatocytes in the CisPt group but not in two Pt(IV)-loaded NPs groups (Fig. 8G), implying severe dose-limiting toxicity associated with the CisPt. These results collectively demonstrate that intraperitoneal injection of Pt(IV)-loaded NPs at a therapeutic dose effectively inhibits the growth of intraperitoneal metastatic tumors of ovarian cancer while showing no significant toxicity to major organs.

4. Discussion

Differing from the biological characteristics observed in hematogenous metastatic tumors, ovarian cancer displays distinctive features, with tumor cells primarily spreading within the peritoneal cavity and exhibiting superficial invasiveness [26]. Nevertheless, the rapid proliferation of ovarian cancer cells, which results in organ compression, along with the frequent development of acquired platinum resistance, contributes to its position as the most fatal gynecological malignancy, with a dismal cure rate of merely 30 %. Therefore, overcoming

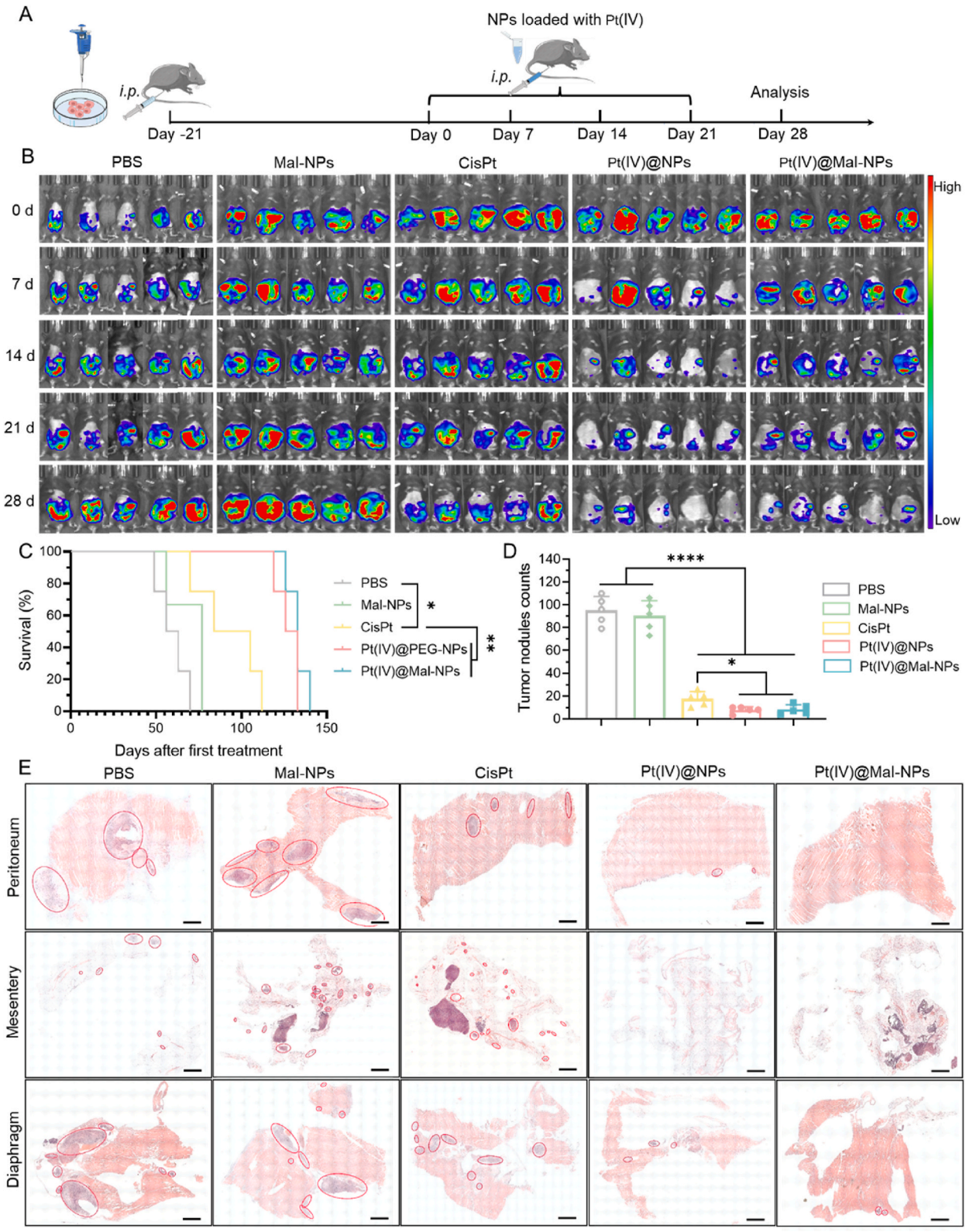

Fig. 6. Antitumor efficacy of Pt(IV)-loaded NPs on mice with peritoneal metastasis ovarian cancer. (A) A schematic diagram is presented to depict the establishment of the peritoneal metastasis tumor model and the procedures of the treatment efficacy study. The doses of CisPt, Pt(IV)@NPs, and Pt(IV)@Mal-NPs were 4 mg/kg body weight per injection, respectively. (B) Bioluminescence images of peritoneal metastasis ovarian cancer in the PBS, Mal-NPs, CisPt, Pt(IV)@NPs, and Pt(IV)@Mal-NPs treatment groups. (C) Monitoring of mice survival (n = 5). (D) Number of abdominal tumor nodules per mouse for each group (n = 5). (E) Representative H&E staining images of the peritoneum, mesentery and diaphragm. The transplanted tumor nodules were indicative by red circles. Scale bar, 1 mm. Data are presented as the means ± SEM. *$p < 0.05$, **$p < 0.01$, ****$p < 0.0001$. (For interpretation of the references to color in this figure legend, the reader is referred to the Web version of this article.)

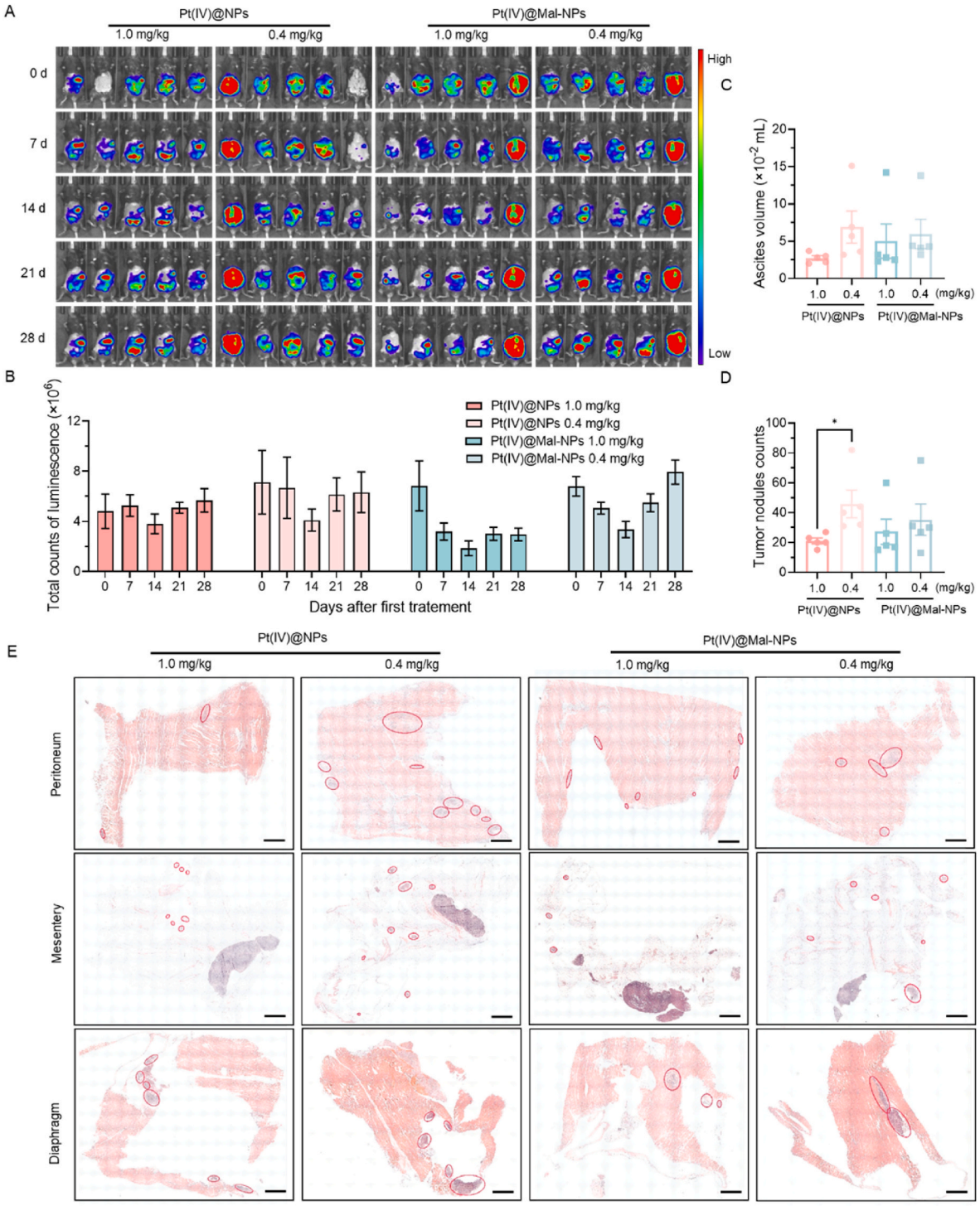

Fig. 7. Differential antitumor efficacy of lower doses of Pt(IV)@NPs and Pt(IV)@Mal-NPs in mice with peritoneal metastasis ovarian cancer. (A) Bioluminescence images of peritoneal metastasis ovarian cancer in mice treated with both doses of Pt(IV)@NPs and Pt(IV)@Mal-NPs. The doses of Pt(IV)@NPs and Pt(IV)@Mal-NPs were 0.4 and 1.0 mg/kg body weight per injection, respectively. (B) Quantification of the average flux luminescence in the abdominal cavity of mice. (C and D) Quantitative analysis of mice ascites (C) and number of abdominal tumor nodules (D) per mouse for each group (n = 5). (E) Representative H&E staining images of the peritoneum, mesentery and diaphragm. The transplanted tumor nodules were indicative by red circles. Scale bar, 1 mm. Data are presented as the means ± SEM. *p < 0.05. (For interpretation of the references to color in this figure legend, the reader is referred to the Web version of this article.)

microtumors following initial treatment to minimize relapse and resistance poses a significant therapeutic challenge in addressing advanced ovarian cancer.

Out of numerous cisplatin analogues, approximately 13 of them have undergone evaluation in clinical trials, with only carboplatin demonstrating substantial advantages over cisplatin and receiving global approval. Although the cytotoxic potency of carboplatin is notably inferior to that of cisplatin its clinical application is still limited by myelosuppression. Pt(IV) prodrugs, as a novel class of platinum-based anticancer agents, have been found to enhance the pharmacological properties of Pt(II)-based anticancer drugs [27]. Their saturated ligands demonstrate greater stability in the bloodstream and reduced systemic

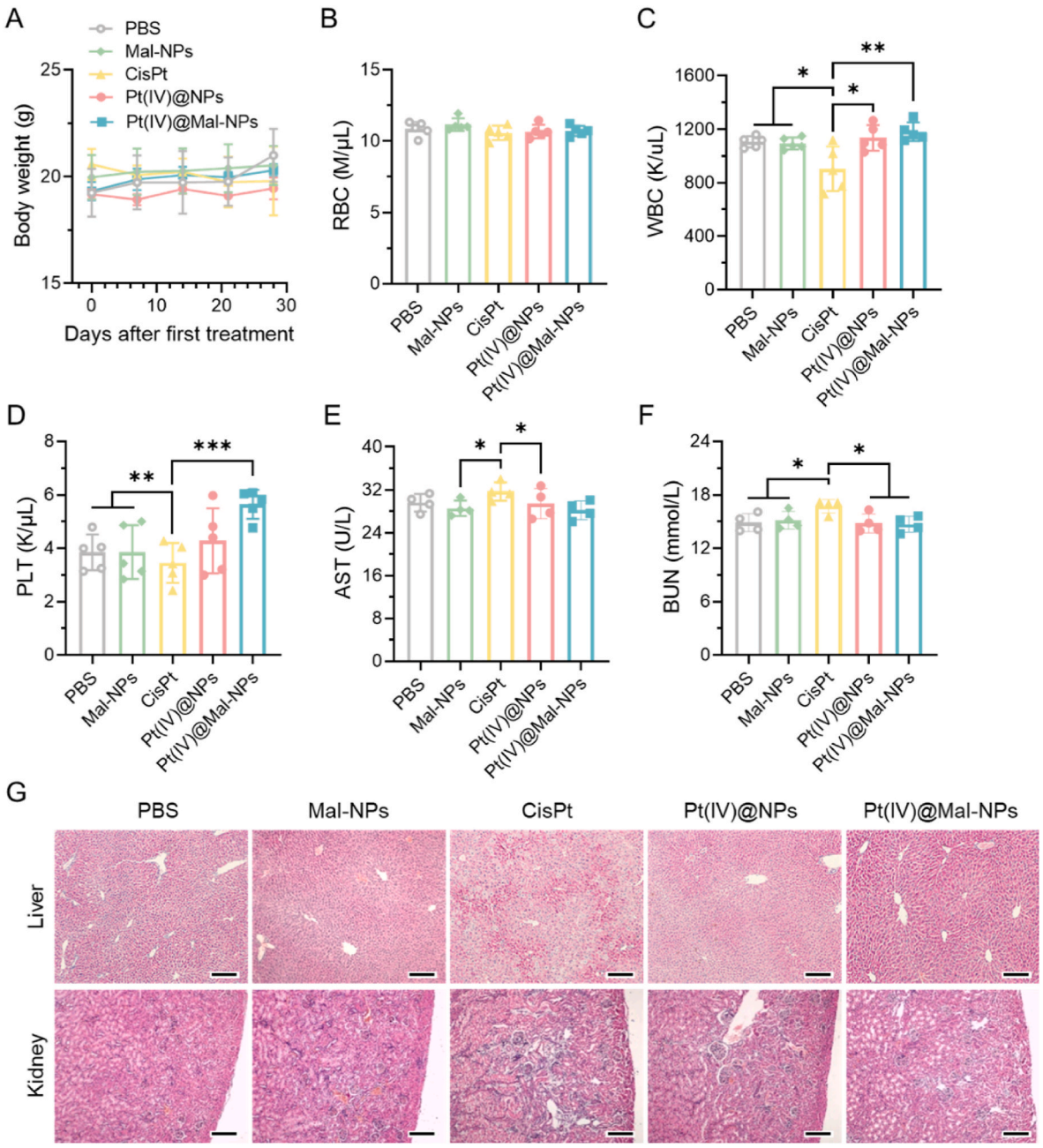

Fig. 8. The effects of Pt(IV)@NPs treatment on major organs (Pt 4 mg/kg body weight per injection). (A) Changes in mouse body weight during treatment with PBS, Mal-NPs, CisPt, Pt(IV)@NPs, and Pt(IV)@Mal-NPs (n = 5). (B - F) Evaluation of RBC (B), WBC (C), PLT (D), and biochemical parameters (E and F) of mice after different treatments (n = 5). (G) Representative H&E staining images of the liver and kidney post-treatment. Scale bar, 500 μm. Data are presented as the means ± SEM. *p < 0.05, **p < 0.01, ***p < 0.001.

organ toxicity. Upon internalized by tumor cells, Pt(IV) prodrugs are selectively activated by high concentrations of the reducing agent GSH, thereby exerting precise cytotoxic effects [28]. However, despite the efficacy and absence of platinum resistance observed in numerous new-generation platinum complexes, their clinical application remains relatively limited. Hence, current research on novel platinum-based drugs should prioritize the identification of methods for targeted drug delivery to tumor sites and the minimization of side effects, rather than solely emphasizing the development of new chemical compounds [29].

The constrained blood supply to peritoneal metastatic tumor nodules hinders the effectiveness of systemic chemotherapy. Intraperitoneal chemotherapy faces the challenge of ensuring drug penetration and retention while minimizing toxicity to non-target areas [30]. Although postoperative IP aerosol delivery (PIPAC) shows potential in extending survival [31], its non-targeted and invasive nature may lead to complications. Current chemotherapy, however, fall short in preventing relapse and eventual death because of three main factors: pharmacokinetics, tumor microenvironment, and cancer cell specificity. Experimental evidence indicates a correlation between the proportion of killed tumor cells and the total drug exposure (calculated as drug concentration × exposure time = area under curve (AUC)) for numerous cytotoxic agents. Factors influencing pharmacokinetics encompass first-pass metabolism, prodrug conversion to active metabolites, renal clearance, hepatic drug metabolism, and tumor vascular distribution [32]. Hence, precise regulation of drug exposure and exposure time in tumor cells throughout these processes constitutes a pivotal approach for augmenting the efficacy of tumor treatment. To achieve this, we developed a nanosized platinum prodrug-based chemotherapy delivery system

using PEG-PLGA-based and Mal-PEG-PLGA-based nanoparticles.

Our study revealed that these NPs, remain predominantly in the abdominal cavity with minimal circulation to major organs. After being entrapped within tumor cells, PLGA-based biodegradable NPs released their contents by eventually incorporating into Golgi-associated vesicles of late endosomes [33]. Particularly those with maleimide end-groups, showed enhanced cellular uptake, increased accumulation, and prolonged retention at tumor sites [34]. This implies that successful modification of PEG end-groups with maleimide in nanocarriers has finely tuned the biological properties of the nanodrugs. Moreover, through intraperitoneal administration, the nanocarriers have acquired tumor cell targeting capabilities and enhanced cellular uptake efficiency [35]. Such enhancement can be attributed to the covalent reaction between the maleimide group and the reactive sulfhydryl groups on cell membranes [36]. This further facilitates the efficient uptake of platinum prodrugs by the cells, and the released drugs are selectively activated within tumor cells due to high concentrations of the GSH [22,37], exerting precise cytotoxic effects. Furthermore, the selective localization of NPs with maleimide end-groups, likely due to their ability to covalently bind with tumor cell membranes in the peritoneum, led to reduced absorption by peritoneal capillaries and lower non-targeted toxicity [38]. The efficient enrichment of the NPs in tumor tissues conferred by the maleimide modification also has the potential to increase the concentration of therapeutic agents. In addition, in the peritoneal metastasis ovarian tumor model, Pt(IV)@Mal-NPs demonstrated a distinctive biodistribution and retention effect. They achieved high concentrations of Pt in tumor lesions widely distributed throughout the peritoneal cavity through direct surface contact, bypassing the peritoneal-plasma barrier and significantly reducing the amount of drug entering major organs. This behavior differed significantly in the in situ ovarian neoplasm model, where NPs were absorbed into the portal circulation through peritoneal capillaries due to the absence of interception by disseminated peritoneal tumors.

To undermine the major limitation of cisplatin, unfavorite biodistribution and severe side effects, our approach to enhance cell internalization and active drug retention is of crucial importance [39]. The GSH-sensitive Pt(IV) prodrug NP design takes advantage of the significantly higher concentration of GSH within cancer cells compared to the extracellular tumor microenvironment [40]. This design aims to protect the loaded platinum drug from activation in non-tumor cells, while utilizing redox reactions within tumor cells to consume GSH and generate active drug forms, thus avoiding detoxification while triggering a cascade of apoptotic processes [23]. In comparison to CisPt, which has a short half-life and limited tumor selectivity, Pt(IV)-loaded NPs demonstrated enhanced tumor accumulation [27]. Once internalized by cells, the NPs rapidly disintegrated and were reduced to active Pt (II) drugs in response to intracellular GSH. This GSH-depleting process effectively reduced thiol-mediated detoxification of the reactivated Pt drugs, resulting in more pronounced inhibition of tumor growth and increased apoptosis [22,41], both *in vitro* and *in vivo*.

Compared to Pt(II) complexes, the development of Pt(IV) prodrugs is primarily driven by their chemical inertness, allowing for controlled release of active Pt(II) specifically in the reducing environment of cancer cells through responsive reduction reactions. The physical encapsulation of platinum complexes within nanocarriers further prevents their interaction with endogenous reductants or nucleophilic reagents *in vivo* [42]. The platinum prodrug NPs, particularly Pt(IV)@Mal-NPs, exhibit significant promotion of apoptosis in both cancer cells and tumor tissues, which is closely associated with to the specific binding of the nanocarriers to tumor cells and the specific activation of the platinum prodrugs within tumor cells.

The efficacy of platinum prodrug nanoparticles in inhibiting the growth of ovarian cancer cell lines is dose-dependent and can be primarily attributed to their high internalization rate, overcoming the dose-limiting nature of platinum-based drugs [43]. This enables precise and efficient delivery of platinum prodrugs to ovarian tumor sites, resulting in maximum therapeutic effects. Unlike cisplatin, the platinum prodrug nanoparticles, particularly Pt(IV)@Mal-NPs in low dose, do not accumulate in the kidneys, instead tend to localize in the peritoneal tumor tissue through surface contact. Even in orthotopic tumor models, where the small volume of local tumor tissue may lead to entry into the bloodstream, they tend to accumulate in the reticuloendothelial organs, as this system is responsible for the blood clearance of NPs of this size [44,45].

Our findings reveal that nanocarriers loaded with Pt(IV) prodrugs exhibit significantly enhanced anticancer activity, both in ovarian cancer cell lines and in mice tumor models, with IC50 values reduced by up to 17.5-fold and a decrease in tumor luciferin imaging intensity by up to 10-fold compared to the CisPt group. Particularly, Pt(IV)@Mal-NPs demonstrate promise for specific tumor absorption, leading to notable tumor growth inhibition, superior tumor apoptosis induction, and reduced toxicity compared to cisplatin. These findings not only highlight the potential of NP drug delivery systems for ovarian cancer treatment but also pave the way for future clinical applications of Pt-based prodrugs in treating ovarian and other abdominal metastatic tumors.

5. Conclusion

Our research represents a significant advancement in ovarian cancer by developing of Pt(IV) prodrug nano-formulations. These formulations, characterized by their optimal morphology and high drug loading, have demonstrated improved peritoneal retention and enhanced uptake in ID8 cells, surpassing the effectiveness of traditional CisPt in tumor inhibition while maintaining safety. In particular, the inclusion of maleimide-modified PEG end-groups in the nanoparticle drug delivery system has significantly improved tumor targeting and enabled a responsive action to the presence of GSH, highlighting their potential as a promising therapeutic platform. This research sets the stage for the development of advanced ovarian cancer treatments, leveraging the unique capabilities of nano-formulated Pt(IV) prodrugs to overcome the limitations of conventional platinum-based chemotherapy.

Funding sources

This study was supported by grants from NSFC [82325029, U22A20156, 32171379], the Interdisciplinary Innovation Project of the First Hospital of Jilin University [2022YYGFZJC008], and the Fundamental Research Funds for the Central Universities, JLU.

CRediT authorship contribution statement

Yiting Bai: Writing – review & editing, Writing – original draft, Visualization, Validation, Methodology, Investigation, Formal analysis, Data curation, Conceptualization. **Zhenpeng Wang:** Software, Investigation, Data curation. **Dongzhen Liu:** Software, Investigation, Data curation. **Xiandi Meng:** Software, Resources, Methodology. **Haorui Wang:** Software, Resources, Methodology. **Meiling Yu:** Software, Resources, Methodology. **Songling Zhang:** Writing – review & editing, Supervision, Project administration, Methodology, Funding acquisition, Conceptualization. **Tianmeng Sun:** Writing – review & editing, Supervision, Project administration, Methodology, Funding acquisition, Conceptualization.

Declaration of competing interest

The authors declare that they have no known competing financial interests or personal relationships that could have appeared to influence the work reported in this paper.

Data availability

Data will be made available on request.

Appendix A. Supplementary data

Supplementary data to this article can be found online at https://doi.org/10.1016/j.mtbio.2024.101131.

References

[1] G.C. Jayson, E.C. Kohn, H.C. Kitchener, J.A. Ledermann, Ovarian cancer, Lancet 384 (9951) (2014) 1376–1388.
[2] A. du Bois, A. Reuss, E. Pujade-Lauraine, P. Harter, I. Ray-Coquard, J. Pfisterer, Role of surgical outcome as prognostic factor in advanced epithelial ovarian cancer: a combined exploratory analysis of 3 prospectively randomized phase 3 multicenter trials: by the Arbeitsgemeinschaft Gynaekologische Onkologie Studiengruppe Ovarialkarzinom (AGO-OVAR) and the Groupe d'Investigateurs Nationaux Pour les Etudes des Cancers de l'Ovaire (GINECO), Cancer 115 (6) (2009) 1234–1244.
[3] Z. Lu, J. Wang, M.G. Wientjes, J.L.S. Au, Intraperitoneal therapy for peritoneal cancer, Future Oncol. 6 (10) (2010) 1625–1641.
[4] S. Dilruba, G.V. Kalayda, Platinum-based drugs: past, present and future, Cancer Chemother. Pharmacol. 77 (6) (2016) 1103–1124.
[5] R. Marullo, E. Werner, N. Degtyareva, B. Moore, G. Altavilla, S.S. Ramalingam, P. W. Doetsch, Cisplatin induces a mitochondrial-ROS response that contributes to cytotoxicity depending on mitochondrial redox status and bioenergetic functions, PLoS One 8 (11) (2013) e81162.
[6] A. Troyano, C. Fernandez, P. Sancho, E. de Blas, P. Aller, Effect of glutathione depletion on antitumor drug toxicity (apoptosis and necrosis) in U-937 human promonocytic cells. The role of intracellular oxidation, J. Biol. Chem. 276 (50) (2001) 47107–47115.
[7] Y. Xuan, H. Wang, M.M. Yung, F. Chen, W.S. Chan, Y.S. Chan, S.K. Tsui, H.Y. Ngan, K.K. Chan, D.W. Chan, SCD1/FADS2 fatty acid desaturases equipoise lipid metabolic activity and redox-driven ferroptosis in ascites-derived ovarian cancer cells, Theranostics 12 (7) (2022) 3534–3552.
[8] K.S. Sivalingam, P. Paramasivan, C.F. Weng, V.P. Viswanadha, Neferine potentiates the antitumor effect of cisplatin in human lung adenocarcinoma cells via a mitochondria-mediated apoptosis pathway, J. Cell. Biochem. 118 (9) (2017) 2865–2876.
[9] J.T. Hartmann, H.-P. Lipp, Toxicity of platinum compounds, Expet Opin. Pharmacother. 4 (6) (2003) 889–901.
[10] T.C. Johnstone, K. Suntharalingam, S.J. Lippard, The next generation of platinum drugs: targeted Pt(II) agents, nanoparticle delivery, and Pt(IV) prodrugs, Chem. Rev. 116 (5) (2016) 3436–3486.
[11] L. Galluzzi, L. Senovilla, I. Vitale, J. Michels, I. Martins, O. Kepp, M. Castedo, G. Kroemer, Molecular mechanisms of cisplatin resistance, Oncogene 31 (15) (2012) 1869–1883.
[12] M. Shen, Y. Wang, T. Bing, Y. Tang, X. Liu, Y. Yu, Alendronate triggered dual-cascade targeting prodrug nanoparticles for enhanced tumor penetration and STING activation of osteosarcoma, Adv. Funct. Mater. 33 (49) (2023).
[13] B. Yu, Y. Wang, T. Bing, Y. Tang, J. Huang, H. Xiao, C. Liu, Y. Yu, Platinum prodrug nanoparticles with COX-2 inhibition amplify pyroptosis for enhanced chemotherapy and immune activation of pancreatic cancer, Adv. Mater. 36 (11) (2024) e2310456.
[14] G. Li, B. Sun, Y. Li, C. Luo, Z. He, J. Sun, Small-molecule prodrug nanoassemblies: an emerging nanoplatform for anticancer drug delivery, Small 17 (52) (2021) e2101460.
[15] C. Luo, J. Sun, B. Sun, Z. He, Prodrug-based nanoparticulate drug delivery strategies for cancer therapy, Trends Pharmacol. Sci. 35 (11) (2014) 556–566.
[16] B. Ahn, J. Park, K. Singha, H. Park, W.J. Kim, Mesoporous silica nanoparticle-based cisplatin prodrug delivery and anticancer effect under reductive cellular environment, J. Mater. Chem. B 1 (22) (2013) 2829–2836.
[17] D.K. Armstrong, B. Bundy, L. Wenzel, H.Q. Huang, R. Baergen, S. Lele, L. J. Copeland, J.L. Walker, R.A. Burger, Intraperitoneal cisplatin and paclitaxel in ovarian cancer, N. Engl. J. Med. 354 (1) (2006) 34–43.
[18] M. Markman, B.N. Bundy, D.S. Alberts, J.M. Fowler, D.L. Clark-Pearson, L. F. Carson, S. Wadler, J. Sickel, Phase III trial of standard-dose intravenous cisplatin plus paclitaxel versus moderately high-dose carboplatin followed by intravenous paclitaxel and intraperitoneal cisplatin in small-volume stage III ovarian carcinoma: an intergroup study of the Gynecologic Oncology Group, Southwestern Oncology Group, and Eastern Cooperative Oncology Group, J. Clin. Oncol. 19 (4) (2001) 1001–1007.
[19] L.B. Wenzel, H.Q. Huang, D.K. Armstrong, J.L. Walker, D. Cella, G. Gynecologic Oncology, Health-related quality of life during and after intraperitoneal versus intravenous chemotherapy for optimally debulked ovarian cancer: a Gynecologic Oncology Group Study, J. Clin. Oncol. 25 (4) (2007) 437–443.
[20] C. Marchetti, C. Pisano, G. Facchini, G.S. Bruni, F.P. Magazzino, S. Losito, S. Pignata, First-line treatment of advanced ovarian cancer: current research and perspectives, Expert Rev. Anticancer Ther. 10 (1) (2010) 47–60.
[21] R. Liu, A.H. Colby, D. Gilmore, M. Schulz, J. Zeng, R.F. Padera, O. Shirihai, M. W. Grinstaff, Y.L. Colson, Nanoparticle tumor localization, disruption of autophagosomal trafficking, and prolonged drug delivery improve survival in peritoneal mesothelioma, Biomaterials 102 (2016) 175–186.
[22] X. Ling, X. Chen, I.A. Riddell, W. Tao, J. Wang, G. Hollett, S.J. Lippard, O. C. Farokhzad, J. Shi, J. Wu, Glutathione-scavenging poly(disulfide amide) nanoparticles for the effective delivery of Pt(IV) prodrugs and reversal of cisplatin resistance, Nano Lett. 18 (7) (2018) 4618–4625.
[23] X. Ling, J. Tu, J. Wang, A. Shajii, N. Kong, C. Feng, Y. Zhang, M. Yu, T. Xie, Z. Bharwani, B.M. Aljaeid, B. Shi, W. Tao, O.C. Farokhzad, Glutathione-responsive prodrug nanoparticles for effective drug delivery and cancer therapy, ACS Nano 13 (1) (2019) 357–370.
[24] G. Zhuang, C. Meng, X. Guo, P.S. Cheruku, L. Shi, H. Xu, H. Li, G. Wang, A. R. Evans, S. Safe, C. Wu, B. Zhou, A novel regulator of macrophage activation: miR-223 in obesity-associated adipose tissue inflammation, Circulation 125 (23) (2012) 2892–2903.
[25] W. Wang, J. Cai, J. Wen, X. Li, Y. Yu, L. Zhang, Q. Han, Z. Wei, Y. Ma, F. Ying, X. Xu, W. Li, Q. Yang, S. Sun, X. He, L. Cai, H. Xiao, Z. Wang, Boosting ferroptosis via abplatin(iv) for treatment of platinum-resistant recurrent ovarian cancer, Nano Today 44 (2022).
[26] E. Lengyel, Ovarian cancer development and metastasis, Am. J. Pathol. 177 (3) (2010) 1053–1064.
[27] C. Zhang, C. Xu, X. Gao, Q. Yao, Platinum-based drugs for cancer therapy and anti-tumor strategies, Theranostics 12 (5) (2022) 2115–2132.
[28] H. Huang, Y. Dong, Y. Zhang, D. Ru, Z. Wu, J. Zhang, M. Shen, Y. Duan, Y. Sun, GSH-sensitive Pt(IV) prodrug-loaded phase-transitional nanoparticles with a hybrid lipid-polymer shell for precise theranostics against ovarian cancer, Theranostics 9 (4) (2019) 1047–1065.
[29] S.A. Abu-Surrah, M. Kettunen, Platinum group antitumor chemistry: design and development of new anticancer drugs complementary to cisplatin, Curr. Med. Chem. 13 (11) (2006) 1337–1357.
[30] W.P. Ceelen, M.F. Flessner, Intraperitoneal therapy for peritoneal tumors: biophysics and clinical evidence, Nat. Rev. Clin. Oncol. 7 (2) (2010) 108–115.
[31] M. Alyami, M. Hübner, F. Grass, N. Bakrin, L. Villeneuve, N. Laplace, G. Passot, O. Glehen, V. Kepenekian, Pressurised intraperitoneal aerosol chemotherapy: rationale, evidence, and potential indications, Lancet Oncol. 20 (7) (2019) e368–e377.
[32] L. Iyer, M.J. Ratain, Pharmacogenetics and cancer chemotherapy, Eur. J. Cancer 34 (10) (1998) 1493–1499.
[33] T. Chernenko, C. Matthäus, L. Milane, L. Quintero, M. Amiji, M. Diem, Label-free Raman spectral imaging of intracellular delivery and degradation of polymeric nanoparticle systems, ACS Nano 3 (11) (2009) 3552–3559.
[34] X. Wang, X. Meng, K. Mao, H. Chen, X. Cong, F. Liu, J. Wang, S. Liu, Y. Xin, G. Zhu, H. Tan, Y.G. Yang, T. Sun, Maleimide as the PEG end-group promotes macrophage-targeted drug delivery of PEGylated nanoparticles in vivo by enhancing interaction with circulating erythrocytes, Biomaterials 300 (2023) 122187.
[35] Z. Li, D. Li, Q. Li, C. Luo, J. Li, L. Kou, D. Zhang, H. Zhang, S. Zhao, Q. Kan, J. Liu, P. Zhang, X. Liu, Y. Sun, Y. Wang, Z. He, J. Sun, In situ low-immunogenic albumin-conjugating-corona guiding nanoparticles for tumor-targeting chemotherapy, Biomater. Sci. 6 (10) (2018) 2681–2693.
[36] S.R. Lee, Critical role of zinc as either an antioxidant or a prooxidant in cellular systems, Oxid. Med. Cell. Longev. 2018 (2018) 9156285.
[37] X.L. Li, Z.Y. Duan, X.T. Chen, D.Y. Pan, Q. Luo, L. Gu, G. Xu, Y.G. Li, H. Zhang, Q. Y. Gong, R.J. Chen, Z.W. Gu, K. Luo, Impairing tumor metabolic plasticity via a stable metal-phenolic-based polymeric nanomedicine to suppress colorectal cancer, Adv. Mater. 35 (23) (2023).
[38] B. Bortot, M. Mongiat, E. Valencic, S. Dal Monego, D. Licastro, M. Crosera, G. Adami, E. Rampazzo, G. Ricci, F. Romano, G.M. Severini, S. Biffi, Nanotechnology-based cisplatin intracellular delivery to enhance chemo-sensitivity of ovarian cancer, Int. J. Nanomed. 15 (2020) 4793–4810.
[39] R. Agarwal, S.B. Kaye, Ovarian cancer: strategies for overcoming resistance to chemotherapy, Nat. Rev. Cancer 3 (7) (2003) 502–516.
[40] E. Perez-Herrero, A. Fernandez-Medarde, Advanced targeted therapies in cancer: drug nanocarriers, the future of chemotherapy, Eur. J. Pharm. Biopharm. 93 (2015) 52–79.
[41] K. Luo, W. Guo, Y. Yu, S. Xu, M. Zhou, K. Xiang, K. Niu, X. Zhu, G. Zhu, Z. An, Q. Yu, Z. Gan, Reduction-sensitive platinum (IV)-prodrug nano-sensitizer with an ultra-high drug loading for efficient chemo-radiotherapy of Pt-resistant cervical cancer in vivo, J. Contr. Release 326 (2020) 25–37.
[42] R. Duncan, Polymer conjugates as anticancer nanomedicines, Nat. Rev. Cancer 6 (9) (2006) 688–701.
[43] M. Sancho-Albero, G. Facchetti, N. Panini, M. Meroni, E. Bello, I. Rimoldi, M. Zucchetti, R. Frapolli, L. De Cola, Enhancing Pt(IV) complexes' anticancer activity upon encapsulation in stimuli-responsive nanocages, Adv. Healthcare Mater. 12 (17) (2023) e2202932.
[44] A.C. Anselmo, S. Kumar, V. Gupta, A.M. Pearce, A. Ragusa, V. Muzykantov, S. Mitragotri, Exploiting shape, cellular-hitchhiking and antibodies to target nanoparticles to lung endothelium: synergy between physical, chemical and biological approaches, Biomaterials 68 (2015) 1–8.
[45] Y.N. Zhang, W. Poon, A.J. Tavares, I.D. McGilvray, W.C.W. Chan, Nanoparticle-liver interactions: cellular uptake and hepatobiliary elimination, J. Contr. Release 240 (2016) 332–348.